PHYSICAL REVIEW B VOLUME 35, NUMBER 5 15 FEBRUARY 1987-I

Epitaxy, overlayer growth, and surface segregation for Co/GaAs(110) and Co/GaAs(100)-$c(8\times2)$

F. Xu, J. J. Joyce, M. W. Ruckman,* H. -W. Chen, F. Boscherini, D. M. Hill, S. A. Chambers, and J. H. Weaver
Department of Chemical Engineering and Materials Science, University of Minnesota, Minneapolis, Minnesota 55455
(Received 15 September 1986)

We present high-resolution synchrotron-radiation core-level photoemission results which show that the room-temperature deposition of Co onto GaAs(110) induces limited substrate disruption, leading to Ga and As intermixing with the metal overlayer. High-energy Auger electron diffraction and low-energy electron diffraction measurements indicate that Co orders weakly to form a metastable, epitaxial bcc matrix with principal crystallographic axes parallel to those of the substrate. Angle-dependent x-ray photoemission results show that the distribution of Ga and As in the Co overlayer varies with, and is dependent on, the Co thickness. Together, these results show that the amount of dissociated Ga and As in the overlayer decays exponentially away from the Co/GaAs interface ($1/e$ length 3 Å); that As surface segregates and its concentration profile is exponential away from the vacuum into the Co overlayer (surface concentration 5.8 at. % at 150-Å Co thickness, $1/e$ decay length 5 Å); and that the As solubility in the Co film far from either boundary is 0.26 at. %. This paper demonstrates that substrate disruption and epitaxial growth are not mutually exclusive provided that the disruption is not too severe and that conditions necessary for epitaxy exist.

INTRODUCTION

The typical boundary regions formed between transition-metal overlayers and semiconductor substrates are characterized by disruption of the semiconductor accompanied by atomic interdiffusion and compound formation. The spatial extend of this boundary region and its heterogeneity depend on the details of the system.[1–8] Likewise, fundamental electronic properties such as the Schottky-barrier height are influenced by defects related to the morphological and chemical conditions at the interface. Unfortunately, there is as yet no clear way to predict the morphology, species profile, and stability of this region. At the same time, the control of interface properties is increasingly important for microelectronic engineering as increased levels of integration are attempted and devices shrink in size. For these applications, the identification of metals that produce highly ordered, stable interfaces is of great importance.

In this paper, we report studies of the room-temperature formation of Co overlayers on cleaved GaAs(110) and on sputter-annealed GaAs(100)-$c(8\times2)$ substrates (both n type with Si doping at 4×10^{18} cm^{-3}). We have used high-resolution synchrotron radiation photoemission, angle-resolved Auger electron spectroscopy, low-energy electron diffraction, and angle-dependent x-ray photoemission to probe the evolving interface as a function of overlayer thickness. The goal of this study was to examine the chemical interactions at the interface, determine the character of the compounds which form (if any), and assess the spatial distribution of the Ga and As atoms which are disrupted from the substrate following Co deposition (if such disruption occurs). Since earlier studies had shown epitaxial bcc Co growth on GaAs,[9–12] we were also interested in characterizing the structure of the Co overlayer at very low coverage. Co/GaAs was felt to be an optimal system in which to combine chemical and structural mapping of the boundary region because disruption of the substrate should be minimal and the profile of the semiconductor atoms in the metal overlayer could be determined.[13,14]

In this paper, we will show that Co does induce limited disruption of the substrate, and thereby promotes Ga and As out-diffusion, but that a template suitable for epitaxy is left intact. The result is the formation of weakly ordered bcc Co. The interface between the undisrupted GaAs surface and the growing Co layer is characterized by an exponentially decreasing amount of Ga and As. At the same time, there is segregated As at the vacuum surface and a characteristic concentration profile away from that surface. The amount of the surface segregated As decreases with Co thickness as the As is dissolved in the increasingly thick Co layer.

EXPERIMENTAL TECHNIQUES

The high-resolution synchrotron radiation photoemission studies were conducted at the Wisconsin Synchrotron Radiation Center using the Grasshopper Mark II beamline + monochromator and a photoelectron spectrometer described in detail elsewhere.[15] For those studies, we used cleaved GaAs(110) and emphasized the developing chemical nature of the interface by following the Ga and As $3d$ core emission as a function of metal overlayer thickness. These measurements optimized surface sensitivity, using photon energies which gave photoelectron kinetic energies of ~36 eV and mean free paths of ~4 Å. These results therefore gave insight into the

 ©1987 The American Physical Society

properties of the outermost ~12 Å of the overlayer.

To gain complementary structural information about the evolving Co overlayer, we undertook angle-resolved Auger electron spectroscopy and low-energy-electron diffraction (LEED) studies. The experimental system allowed measurement of Co *LMM* Auger emission as a function of solid angle of detection,[16] as well as LEED *I-V* curves at a fixed scattering angle in any desired azimuthal plane. The angular resolution for these measurements was $\Delta\theta\Delta\phi = 2°\times 4°$. For these experiments, we used GaAs(100) wafers which were Ar^+-ion sputtered and annealed *in situ* to obtain the $c(8\times 2)$ surface reconstruction. The cleaning procedures for these experiments involved ultrasonic rinsing in acetone and methanol, etching in a solution of H_2SO_4:H_2O_2:H_2O (5:1:1 by volume), and rinsing in methanol and water to remove organic contaminants. The wafers were then dried and mounted on the sample goniometer. Once in UHV, we cleaned the surface by cycles of Ar^+ sputtering at 500 eV and simultaneous annealing (~400 °C) during Ar^+ bombardment (~150 V). Finally, the sample was annealed at 490 °C for 30 min to form the Ga-rich GaAs(100)-$c(8\times 2)$ surface.

A third set of measurements was undertaken using angle-dependent x-ray photoelectron spectroscopy with a photon energy of 1486.6 eV. These studies sought to determine the spatial distribution of the Ga and As atoms in the evolving overlayer, with emphasis on the profile near the surface. For these measurements we again used wafers, following the cleaning procedures described in the previous paragraph. The x-ray photoelectron spectroscopy (XPS) measurements were performed using a Surface Science Instruments SSX-100-03 x-ray photoelectron spectrometer appended to a dual chamber UHV spectrometer designed for *in situ* interface preparation and polar-angle-resolved spectral measurements.[17] All XPS data were obtained with a 300-μm monochromatized x-ray beam diameter and a pass energy of 50 eV. The half angle of the analyzer cone of acceptance was 15°.

Each of the three spectrometers had an operating pressure of $\sim 5\times 10^{-11}$ Torr. Cobalt was evaporated resistively from tungsten boats placed ~30 cm from the GaAs targets. Extensive degassing of the Co sources made it possible to form the interface at pressures better than 2×10^{-10} Torr, consistent with the need to maintain ultraclean conditions. Typical deposition rates were ~1 Å per minute, as measured with calibrated Inficon quartz oscillators placed near the samples. All depositions and studies were conducted at room temperature. In this paper, we use angstrom units for the nominal Co coverage; 1.4 Å = 1 monolayer (ML) of Co in a structure commensurate with the GaAs(100) substrate since the Co atom density is twice that of the template. The surface atom density is 6.26×10^{14} atoms/cm^2 for GaAs(100) and 8.9×10^{14} atoms/cm^2 for GaAs(110).

RESULTS AND DISCUSSION

A. Interface chemistry

In Fig. 1 we show representative Ga and As 3*d* core-level energy distribution curves (EDC's) for Co/GaAs(110). These synchrotron radiation photoemission spectra have been background subtracted and normalized to highlight changes in line shape induced by the deposition of Co. Photon energies of 60 and 85 eV were chosen for the Ga and As cores, respectively, to give maximum surface sensitivity (95% of the signal comes from within 3λ of the surface where λ is the photoelectron mean free path of ~4 Å). Band-bending-induced shifts of both the Ga and As core levels have been removed by aligning the substrate core-level components. The bottommost EDC's of Fig. 1 are for the clean surface where emission from surface atoms (labeled *s*) is shifted 0.28 eV to higher binding energy for Ga and 0.38 eV to lower binding energy for As.[18] The overall experimental resolution (photons plus electrons) was 208 meV for Ga and 262

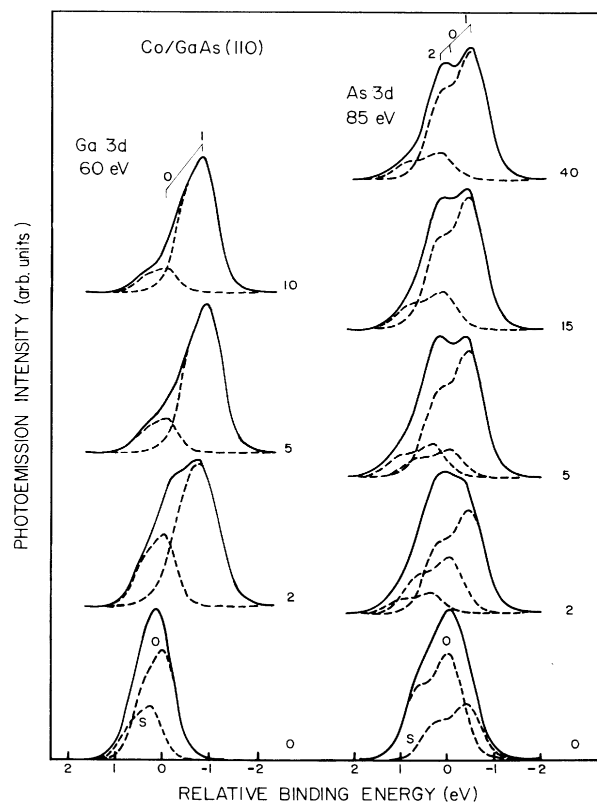

FIG. 1. Representative Ga and As 3*d* core-level energy distribution curves showing the line-shape evolution with Co coverage. These photon energies result in very high surface sensitivity (~4 Å photoelectron mean free path). The bottom pair of curves are for the clean surface showing both substrate (0) and surface shifted (*s*) emission. For Ga, a chemically shifted feature, labeled 1, appears at lower binding energy and shifts away from the substrate line with increasing coverage (total shift −0.9 eV). For As, the Co-induced components, labeled 1 and 2, have distinct binding energy shifts of −0.45 and +0.25 eV relative to the substrate. For both Ga and As, component 1 corresponds to dissolved atoms in the Co matrix. For As, component 2 corresponds to atoms which are incompletely coordinated with Co on the Co surface.

meV for As.

Room temperature intermixing of Ga and As with the as-deposited Co overlayers is evident from Fig. 1 through examination of the evolving $3d$ core-level emission. For Ga, a shoulder appears at subangstrom metal coverages on the lower binding-energy side of the Ga $3d$ line opposite the surface-shifted component (not shown, but see Ref. 13 for low-coverage results for Fe/GaAs). At the same time, the surface component diminishes rapidly. From the results for coverages of 2, 5, and 10 Å shown in Fig. 1, we see that the chemically shifted feature moves to lower binding energy with increasing metal coverage, stabilizing at 0.9 eV lower binding energy than Ga in GaAs. Even for coverages as low as 2 Å the chemically shifted component is dominant, indicating that disruption of the substrate has produced significant amounts of intermixed Ga in the overlayer. Analysis of the total Ga $3d$ emission normalized to that of the cleaved surface shows that the Ga content of the probed region attenuates quickly with coverage. By the time that 20 Å of Co have been deposited onto GaAs(110), it is no longer possible to detect Ga within the probe depth (outermost ~ 12 Å). At somewhat lower coverages, the results show that all of the Ga is in an intermixed environment and is fully dilute. There is no evidence for surface segregated Ga.

Ga $3d$ line-shape decompositions were undertaken to investigate the changing chemical environment of the Ga atoms, and typical decompositions are shown as dashed lines in Fig. 1. To obtain these fits, we performed computer decompositions of the total emission using Voigt functions. For all Ga spectra, the spin-orbit splitting was held at 453 meV and the branching ratio was 0.61. The fixed Lorentzian width of 155 meV was determined by self-consistent calculations of the spectra for the cleaved surface and is in excellent agreement with those obtained by Miller and Chiang.[18] A Gaussian linewidth of 208 meV was used for the substrate to represent the total instrument response. This resolution was in excellent agreement with design parameters for the monochromator (based on slits widths, grating line density, and grating radius of curvature) and the electron energy analyzer (pass energy 10 eV). For the reacted component the Gaussian width and the binding energy were allowed to vary to account for inequivalent Ga sites and the observed steady shift in binding energy. The smooth variation in energy of the Ga $3d$ core level indicated, moreover, that a Co-Ga solution formed rather than a specific bonding configuration, and the analysis indicated a line shape sharpening for the reacted Ga component as the metal thickness increased. This Ga behavior is analogous to that observed for several other transition-metal—GaAs systems (Refs. 1, 3—5, 7, 8, 13, and 19). In the discussion of the angle-resolved XPS results, we will show that the Ga concentration decreases approximately exponentially with distance from the GaAs surface ($1/e$ length ~ 3 Å).

Comparison of the results of Fig. 1 for Co/GaAs with those for Fe/GaAs (Ref. 13) shows that the substrate component attenuates more rapidly for Co overlayers, consistent with thermodynamic predictions of greater Co-Ga interaction compared to Fe-Ga.[20] As a result, there appears to be a greater tendency for substrate disruption. Examination of the Ga $3d$ core-level behavior for many other metal-GaAs systems shows that the total Ga core-level binding-energy shifts vary directly with the Pauling electronegativity difference between the overlayer and Ga.[19]

In Fig. 1 we also show representative As $3d$ core-level EDC's and their decompositions. For the fitting, we used Lorentzian widths of 172 meV, a spin-orbit splitting of 695 meV, and a branching ratio of 0.63. The Gaussian widths for the substrate and the chemically shifted components were initially allowed to vary, but consistently converged to 262 meV. This Gaussian width is again in excellent agreement with the predicted resolution at 85-eV photon energy. For As decomposition, the surface As core level at -0.38 eV overlaps with the chemically shifted component at -0.45 eV and, at submonolayer coverage, it is difficult to unambiguously separate the diminishing surface atom contribution from the increasing reacted-As contribution. Indeed, we observed little or no line-shape change for 0.5-Å coverage. Insight into the rate of loss of surface contribution could be gained, however, by comparing with the submonolayer behavior for Ga where the surface shift was $+0.28$ eV. By 1- and 2-Å Co coverage, emission grew on the low binding-energy side of the substrate component, labeled 1 in Fig. 1, and provided clear evidence for intermixed As. At higher coverage this shifted component dominated the EDC's.

In line-shape analysis of these families of curves we found that adequate fits could not be obtained with only two components. Inspection of the raw data at high coverage shows that this might have been expected because of the anomalous As $3d$ branching ratio. When a third component is introduced, labeled 2 in Fig. 1, the agreement is excellent and internally consistent. The binding energies for the two chemically shifted components were -0.45 and $+0.2$ eV. The component at higher binding energy can be associated with As atoms *on* the Co surface, while the component shifted to lower binding energy corresponds to As in solution *within* the Co matrix and coordinated by Co. Depending on the coverage, the XPS results detect the dissolved atoms at the interface (low coverage) or near the surface (high coverage). Analogous surface atom emission had, in fact, been observed for Fe/GaAs but, because of the way the decompositions were done, the distinction was not sufficiently clear.[21] Previous angle-dependent XPS and Auger studies of Fe/GaAs did provide evidence for As enrichment of the surface region but again could not distinguish As atoms on the surface from those dissolved within the Co matrix. The present polar-angle-dependent XPS results make it possible to determine the surface concentration of these atoms and the exponential decay of As concentration into the Co film.

In Fig. 2 we show attenuation curves for Ga and As $3d$ emission intensities as a function of cobalt thickness, defined as $\ln[I(a)/I(0)]$, where a is the coverage. The total intensities are shown as solid lines, and the dashed curves for the different components were obtained from the core-level decompositions. The total rate of attenuation is much faster for Ga than for As and the As emission persists to high coverage. Component-specific profiles show that the rates of attenuation of substrate Ga and As are

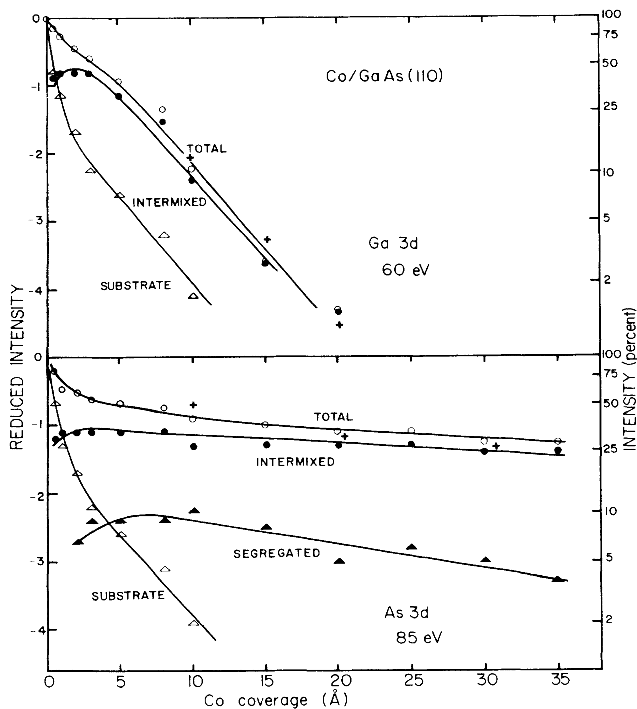

FIG. 2. Normalized attenuation curves using the results of Fig. 1 to show the rate of change of the As and Ga content of the probed region as a function of Co coverage. For Ga, the substate emission diminishes rapidly due to disruption at low coverage and covering up at higher coverage (open triangles). The amount of Ga dissolved in the Co matrix likewise diminishes exponentially after ~5 Å coverage, indicating very limited out-diffusion. For As, the substrate emission is the same as that for Ga. The solid triangles correspond to As on the free surface and the solid circles correspond to As coordinated with Co in solution near the interface (at low coverage) and in the segregated region close to the free surface (at high coverage). The + symbols are predicted total intensities based on the atomic profile shown in Fig. 8.

equal with $1/e$ values of ~1 Å at the earliest stages of formation because substrate disruption has the effect of increasing the distance from the undisturbed substrate and the surface. By ~3 Å, the decay is slower ($1/e$ value of ~4 Å), consistent with photoelectrons propagating through an epitaxially growing overlayer (basically layer-by-layer formation discussed in the following section). Further, Fig. 2 shows that for coverages exceeding 5 Å, the emission from the disrupted atoms also diminishes exponentially with the same $1/e$ length as the substrate. From Fig. 1 we therefore see that the environment of the disrupted Ga atoms becomes increasingly dilute as Ga enters the Co-derived overlayer in solution form. The results of Fig. 2 show that Ga is unable to diffuse away from the interface, and is covered up by further metal deposition.

Our photoemission results reveal that the As behavior is very different from that of Ga because emission from the intermixed and surface segregated components, which have distinct binding energies, persists with little attenuation as the Co overlayer grows. Since there is no evidence of extended disruption of the substrate after it is covered up, we propose that our surface sensitive measurements reveal As atoms which have been disrupted at the early stages of deposition and are only partially trapped at the interface. These atoms form weak bonds with Co and can be displaced by Co atoms in favor of the formation of epitaxial bcc Co. They could also be incorporated into the Co matrix, although the solubility of As in Co is low (but not zero). Most are therefore displaced to the surface where they are only partially coordinated with Co (chemical shift +0.2 eV). The concentration profile near the surface is not a step function and, instead, the amount of As decays into the bulk. The As atoms in the Co matrix are fully coordinated with Co (chemical shift −0.45 eV). This process continues as the Co layer is built up. The angle-dependent XPS studies at high coverage make it possible to quantitatively determine the As profile.

B. Structure of the overlayer

In order to investigate the structure of the overlayer, we have employed Auger electron diffraction and low-energy electron diffraction (LEED). The purpose here was to determine the extent to which epitaxial bcc Co could form while accommodating the disrupted Ga and As atoms. In Fig. 3 we show LEED I-V curves at a fixed scattering angle of 138° (180°−42°) in two high-symmetry azimuthal planes separated by 45°. The (010) plane is arbitrarily assigned as $\phi=0°$ and $(\bar{1}10)$ is at $\phi=45°$. Using the Bragg condition, we can assign elastic peak intensity maxima to particular diffracted beams. The intense peak in the clean surface curve at $\phi=0°$ is assigned to the (21) beam from the unreconstructed GaAs substrate. Similarly, the lowest-energy peak in the clean surface curve at $\phi=45°$ is assigned to the (11) substrate beam. The additional features in the latter curve result from the $c(8\times2)$ reconstruction. Upon the addition of 0.7 Å (one monolayer) of Co, the diffracted beams from the substrate weaken significantly and remain weak at higher coverages. At 3.5 Å, a peak appears at 48 eV and $\phi=0°$ which is assigned to the (10) beam of bcc Co. The appearance of this beam in the (010) azimuthal plane indicates that bcc Co patches oriented parallel to the substrate surface have grown by a coverage of 3.5 Å (2.5 ML). However, the background is high and the two other LEED beams expected from bcc Co [the second-order (10) beam at 168 eV in (010) and the first-order (11) beam at 84 eV in $(\bar{1}10)$] are very weak. Thus, the LEED data suggest that a weakly ordered bcc phase of Co has grown. These results are in contrast to analogous data for the Fe/GaAs(001) system,[14] which indicated the formation of a well-ordered bcc Fe overlayer by a coverage of 1.5 ML of bcc Fe.

In Fig. 4 we present Co $L_3M_{4,5}M_{4,5}$ Auger diffraction curves in which the polar angle is varied in the (010) azimuthal plane for a range of coverages. In all cases the diffraction curves are qualitatively similar to those which were observed and analyzed in detail for the Fe/GaAs(001) system.[14] However, the present anisotro-

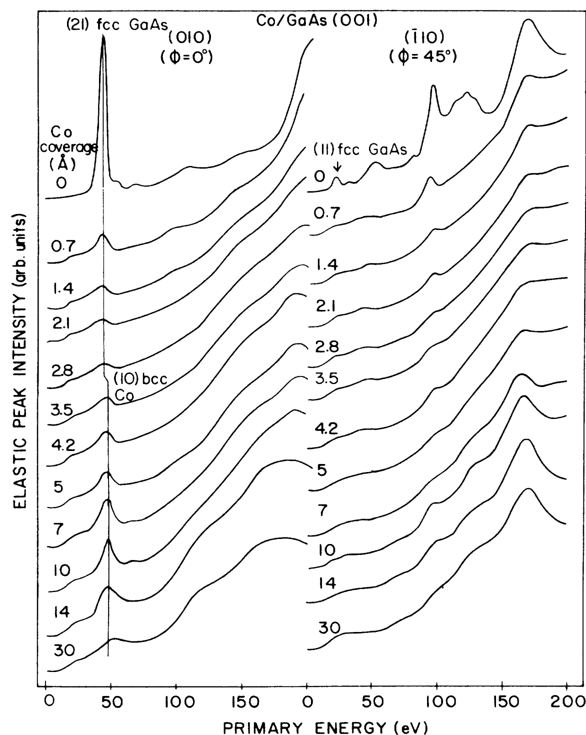

FIG. 3. LEED I-V curves for the Co/GaAs(001) interface in various stages of development. The scattering angle was held fixed at 138°, the sample was oriented for normal electron beam incidence, and I-V curves were collected in two high-symmetry azimuthal planes. The appearance of weak beams associated with the formation of bcc Co at a coverage of 3.5 Å (the equivalent of 2.5 ML of bcc Co) demonstrates that weakly ordered Co clusters grow in registry with the substrate.

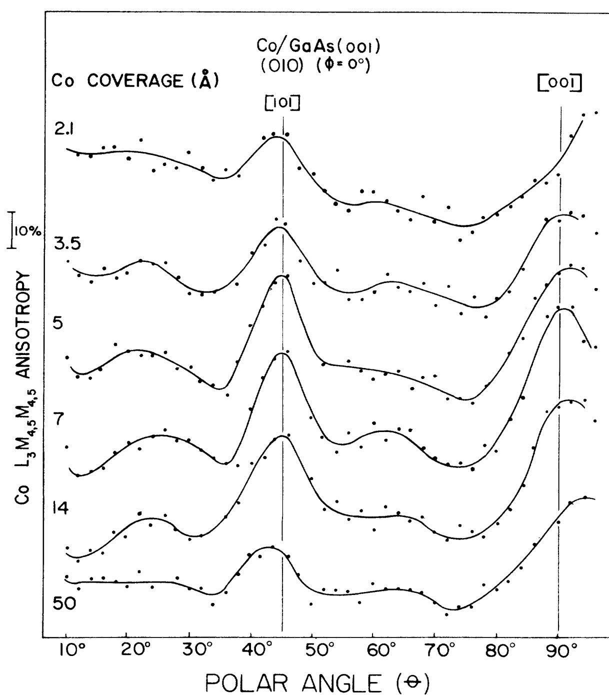

FIG. 4. Co $L_3M_{4,5}M_{4,5}$ polar angular distributions in the (010) azimuth for the Co/GaAs(001) interface as a function of coverage. The weak diffraction induced features at 45° and 90° indicate that weakly ordered Co clusters have formed with limited amounts of substrate atoms occupying face centered interstitial sites. The excitation energy was 5 kV.

pies are much weaker, providing additional evidence for a lower degree of structural order in the Co overlayer relative to the Fe overlayer. For both systems, diffraction maxima occur along the [101] and [001] directions, corresponding to forward scattering along chains of atoms. However, in the case of Fe/GaAs(001), the strength of the peak along [101] could not be fully accounted for with a pure bcc Fe structure. Rather, it was necessary to postulate the presence of impurity atoms in face-centered sites of the bcc structure to provide sufficiently strong scattering along [101]. Indeed, kinematical scattering calculations of the polar-angular distribution in (010) for 10 ML of Fe on GaAs(001) showed excellent agreement with experiment *only* when additional scatterers were placed at the face-centered sites. We concluded that those atoms were outdiffused Ga and As. The qualitative similarities between the Fe/GaAs results and those presented here lead us to believe that a similar phenomenon is occurring, although the intensity of the feature along [101] relative to that along [001] is lower in the present case than for Fe/GaAs(001). This result may indicate a smaller number of substrate atoms in face-centered sites per unit volume for Co/GaAs than for Fe/GaAs.

Our results show that weakly ordered bcc Co forms, quite possibly in the form of similarly oriented crystallites separated by low-angle grain boundaries. The formation of the overlayer is not strictly layer-by-layer since we found evidence for the existence of second-layer atoms before the first layer was complete. [The (21) substrate LEED beam persisted up to a coverage of 2.8 Å or the equivalent of 2 ML of bcc Co.] The result of the coalescing of the patches is that there are two means by which Ga and As can be accommodated in the overlayer near the substrate, namely in the grain boundaries and in the interstices. In the next section, we determine the equilibrium concentration of Ga and As in the matrix.

The structural regularity of the Co overlayer on the (100) face of GaAs is not as high as that reported by Prinz[10] on the (110) surface. The difference may be due to the extensive $c(8\times2)$ reconstruction of the (100) surface. Although the structure of this surface is not yet known, it is believed that covalent bonding between dangling sp^3 surface bonds causes significant distortions in the surface layer and that this affects the structure of the next few deeper layers. Such a reconstructed surface may not provide a template suitable for driving the Co into a metastable bcc phase as well as does the relaxed (110) surface. As Prinz has shown, the lattice parameter versus

composition curve for the Co-Fe system predicts that metastable bcc Co would have a lattice constant of ~ 2.82 Å, which is within 0.02% of that of GaAs.[10] Therefore, the (110) surface with its minimal distortion from the ideal bulk GaAs structure evidently induces the formation of a bcc Co phase which is highly ordered. The inability of the (100)-$c(8\times2)$ to do the same way may be a result of the more extensive atomic displacements in the first several layers.

C. Distribution of As and Ga atoms in the Co overlayer

In order to quantitatively determine the spatial distribution of Ga and As normal to the interface, we performed angle-dependent x-ray photoelectron spectroscopy measurements in which the polar angle was varied from grazing to normal emission. By changing the polar angle of emission θ, it was possible to vary the thickness of the region which was sampled, $\sim 3\lambda\sin\theta$, where $\lambda = 17$ Å for photoelectrons of these kinetic energies.

In Fig. 5 we show Ga and As $3d$ XPS spectra at two different polar angles for a 30-Å Co coverage. The dashed curves show decompositions of the total emission based on the line shape of the clean surface. For these decompositions, the overall resolution was about 0.9 eV and it was not possible to distinguish the subtle chemical shifts discussed above. Instead, each spectrum has been fit to a pair of doublets corresponding to the substrate and outdiffused species. For As this procedure was most reliable at coverages for which the substrate could no longer be detected. The results of Fig. 5 demonstrate that the amount of substrate material within the profiling depth of the measurement increases relative to the quantity which has outdiffused as the polar angle is increased from 45° to 90°. These results, and those taken at other coverages (15–150 Å) and other angles (10°–90°), form the basis for assessing the distribution of outdiffused Ga and As atoms in the Co overlayer, as described below.

In Fig. 6 we present reduced total Ga and As $3d$ emission intensities which are analogous to the surface sensitive results of Fig. 2. These results show the difference of attenuation rates due to the change in sampling depth. For Ga the intensity detected at any angle decreases rapidly with coverage. For As the rate decreases only slightly with increasing coverage, indicating the persistence of segregated As. These high-coverage, long-mean-free-path data are in agreement with, and are complementary to, the synchrotron radiation results. (The solid lines drawn in Fig. 6 are predicted attenuation curves to be discussed shortly.)

In Fig. 7 we plot the normalized Ga $3d$ emission relative to the total detected intensity (the sum of the As $3d$, the Ga $3d$, and the Co $3p$ emission) as a function of polar angle θ for several coverages. Each intensity is an integration of the appropriate core-level photoelectron peak after background subtraction. Normalization of the emission intensities has been done by determining the Co $3p$ emission for a thick Co film and the Ga and As $3d$ emission for the GaAs(100) surface under identical measurement conditions (spot size, x-ray intensity, pass energy of the analyzer, detection geometry). This procedure takes into account the photoionization cross sections and the

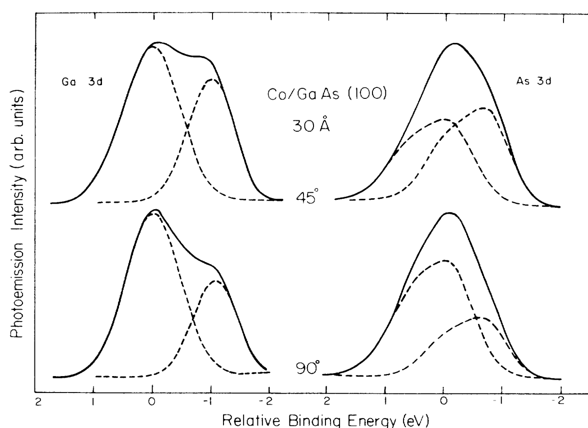

FIG. 5. Polar-angle-dependent x-ray photoemission spectra for the Ga and As $3d$ core levels after the deposition of 30 Å of Co onto GaAs(100). The changes in line shape reflect variations in the probe depth, given by $\lambda\sin\theta$, for angles of 45° and 90°. For these spectra, the mean free path is far greater than that of Fig. 1 (17 Å vs 4 Å).

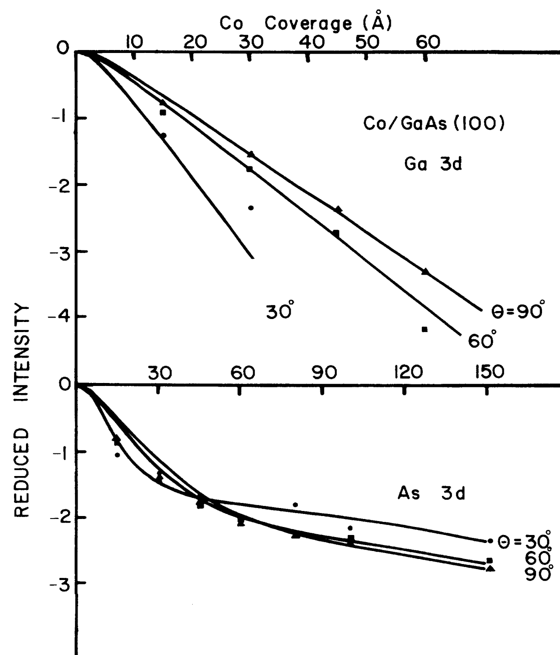

FIG. 6. Ga and As $3d$ emission intensities obtained from the polar-angle-dependent XPS spectra showing the variation in atom concentration sensed as a function of probe depth. The angle of emission of each family of points is indicated. The solid lines were calculated from the distribution function of Fig. 8. For As, the results show surface segregation; for Ga, they show rapid decay with distance from the interface.

analyzer response function and eliminates the reliance on calculated cross sections or results from other experimental systems. As shown in Fig. 7, the relative amount of Ga in the near-surface region is much less than that closer to the interface, as evidenced by the decrease in the ratio at shallow angles. These results confirm that gallium atoms are concentrated close to the interface where intermixing occurs and that the diffusion length of Ga into the overlayer is short.

In Fig. 7 we also show the polar-angle-resolved total intensity of As $3d$ emission relative to the total Ga, As, and Co intensities at high coverages where the Ga content is negligible and there is no contribution from the substrate. A strong As $3d$ signal is easily detected at coverages as high as 150 Å. The percentage of As increases as θ decreases, indicative of segregation of As in the surface and near-surface region,in contrast to the Ga case.

We have fit the data points in Figs. 6 and 7 to a simple continuum model in which the overlayer is treated as a uniform slab which attenuates the photoelectron intensity from atoms contained therein. The photoemission intensity resulting from element A distributed within this slab detected at an angle θ with respect to the surface is given by

$$I_A(\theta)=\sigma_A I_0(\theta) S \int_0^\infty \rho_A(z) e^{-z/\lambda \sin\theta} dz \equiv \sigma_A I_A^0(\theta) \ . \quad (1)$$

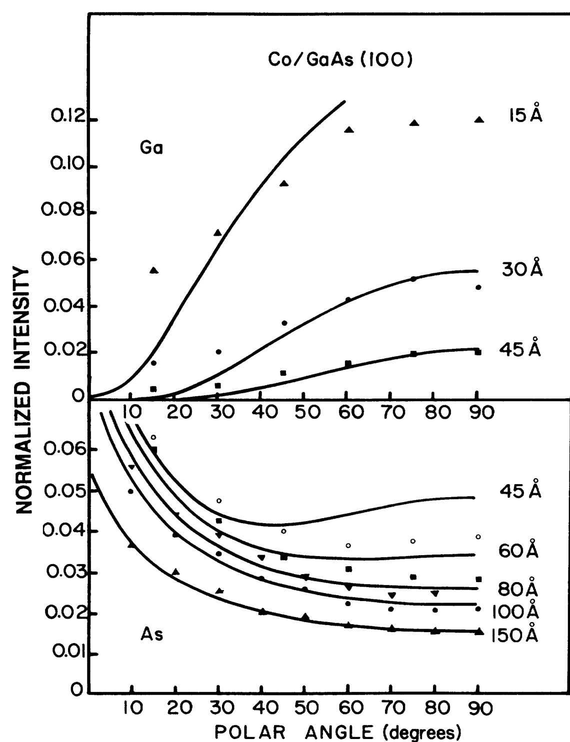

FIG. 7. Normalized Ga $3d$ intensity, $I_{Ga}/(I_{Ga}+I_{As}+I_{Co})$ as a function of detection angle θ for Co coverages of 15, 30, and 45 Å. The solid lines are the fits based on Eq. (4). Corresponding results for As are shown at coverages of 80, 100, and 150 Å, with fits based on Eq. (7).

ρ_A is the density distribution function of element A; σ_A is its photoionization cross section; λ is the inelastic mean free path for the photoelectrons; S is the spot size of the incident x-ray beam; $I_0(\theta)$ is the intensity detected at an angle θ of a pure material with both yield and density equal to one; and z is the distance measured relative to the free surface.

To extract distribution information from polar-angle-resolved photoemission intensities, it is necessary to assume a particular form of $\rho(z)$. The model we present here requires that the reaction between the deposited Co and the substrate is fully completed by the coverage of interest. Hence, Co deposition does not change the quantities of disrupted Ga or As in the Co overlayer. From the above discussion, we know that this coverage is very low, 1–2 Å, and does not significantly restrict the model. In a first approximation, we assume that the GaAs substrate acts as an infinite source of Ga and As and that Co does not diffuse into the substrate.

The density distribution that leads to the most satisfactory fitting of the Ga profiles of Fig. 7 is shown in Fig. 8 and can be written as

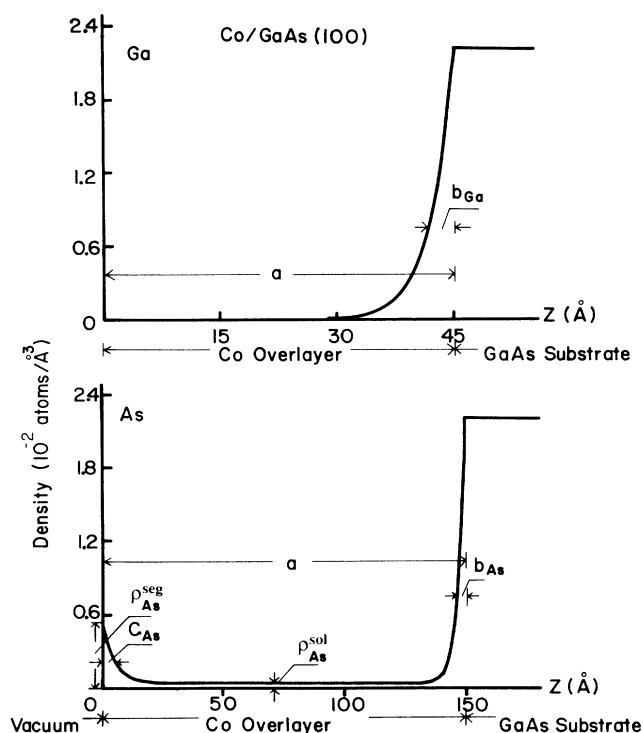

FIG. 8. Distribution functions for Ga and As at coverages of 45 and 150 Å. For Ga, the assumed form is given by an exponential decay into the Co overlayer from the GaAs substrate ($1/e$ length corresponding to $b_{Ga}=3$ Å). For As, the results indicated the need for surface segregation. The concentration on the free surface decreased with coverage. At any coverage, its decay into the Co layer from the free surface could be characterized by another exponential function. Far from either boundary, the As solubility is 0.26 at. %.

$$\rho_{\mathrm{Ga}}(z)=\begin{cases}\rho_{\mathrm{Ga}}^{0}e^{(z-a)/b_{\mathrm{Ga}}} & \text{for } z<a,\\ \rho_{\mathrm{Ga}}^{0} & \text{for } z\geq a,\end{cases} \tag{2}$$

where a is the thickness of Co overlayer, b_{Ga} is a fitting parameter which is the characteristic decay length for the Ga density into the overlayer, and $\rho_{\mathrm{Ga}}^{0}=0.022\,18$ atoms/Å^3 is the Ga bulk density in GaAs. The Ga intensity can be obtained from Eq. (1) as

$$\begin{aligned}I_{\mathrm{Ga}}(\theta)&=\sigma_{\mathrm{Ga}}I_{\mathrm{Ga}}^{0}(\theta)=\sigma_{\mathrm{Ga}}I_{0}(\theta)S\int_{0}^{\infty}\rho_{\mathrm{Ga}}(z)e^{-z/\lambda\sin\theta}dz\\ &=\sigma_{\mathrm{Ga}}I_{0}(\theta)S\lambda\sin\theta\rho_{\mathrm{Ga}}^{0}\{[b_{\mathrm{Ga}}/(\lambda\sin\theta-b_{\mathrm{Ga}})][e^{-a/\lambda\sin\theta}-e^{-a/b_{\mathrm{Ga}}}]+e^{-a/\lambda\sin\theta}\}\ .\end{aligned} \tag{3}$$

To model the As distribution, we assumed the profile shown in Fig. 8 for 150 Å coverage and given by

$$\rho_{\mathrm{As}}(z)=\begin{cases}\rho_{\mathrm{As}}^{\mathrm{seg}}e^{-z/c_{\mathrm{As}}}+\rho_{\mathrm{As}}^{\mathrm{sol}}+\rho_{\mathrm{As}}^{0}e^{(z-a)/b_{\mathrm{As}}} & \text{for } z<a,\\ \rho_{\mathrm{As}}^{0} & \text{for } z\geq a.\end{cases} \tag{4}$$

Here, ρ_{As}^{0} is the As density in GaAs. The term $\rho_{\mathrm{As}}^{0}\exp[(z-a)/b_{\mathrm{As}}]$ again describes the intermixed region near the interface. $\rho_{\mathrm{As}}^{\mathrm{seg}}\exp[-z/c_{\mathrm{As}}]$ describes the profile decaying into the Co layer from the vacuum surface, starting with a surface concentration $\rho_{\mathrm{As}}^{\mathrm{seg}}$. The constant $\rho_{\mathrm{As}}^{\mathrm{sol}}$ represents the small amount of dissolved As far from either boundary. For high coverages, we impose the condition that the total quantity of As segregated to the surface and in solution in Co be constant for all the coverages, i.e.,

$$\int_{0}^{a}(\rho_{\mathrm{As}}^{\mathrm{sol}}+\rho_{\mathrm{As}}^{\mathrm{seg}}e^{-z/c_{\mathrm{As}}})S\,dz=A=\text{const}\ , \tag{5}$$

so that in the limit of $a\gg c_{\mathrm{As}}$ and $a\gg b_{\mathrm{As}}$ (thick Co film with thin intermixed boundary regions) we have $\rho_{\mathrm{As}}^{\mathrm{seg}}=(A/S-\rho_{\mathrm{As}}^{\mathrm{sol}}a)/c_{\mathrm{As}}$. Using the distribution function of Eq. (4), we obtain from Eq. (1)

$$\begin{aligned}I_{\mathrm{As}}&=\sigma_{\mathrm{As}}I_{\mathrm{As}}^{0}(\theta)=\sigma_{\mathrm{As}}I_{0}(\theta)S\int_{0}^{\infty}\rho_{\mathrm{As}}(z)e^{-z/\lambda\sin\theta}dz\\ &=\sigma_{\mathrm{As}}I_{0}(\theta)S\lambda\sin\theta\{[\rho_{\mathrm{As}}^{\mathrm{seg}}c_{\mathrm{As}}/(\lambda\sin\theta+c_{\mathrm{As}})][1-e^{-a[(1/c_{\mathrm{As}})+(1/\lambda\sin\theta)]}]+\rho_{\mathrm{As}}^{\mathrm{sol}}(1-e^{-a/\lambda\sin\theta})\\ &\qquad+[(\rho_{\mathrm{As}}^{0}b_{\mathrm{As}})/(\lambda\sin\theta-b_{\mathrm{As}})][e^{-a/\lambda\sin\theta}-e^{-a/b_{\mathrm{As}}}]+\rho_{\mathrm{As}}^{0}e^{-a/\lambda\sin\theta}\}\ .\end{aligned} \tag{6}$$

As noted above, we can take the overlayer Co layer to have the density of bulk Co, $\rho_{\mathrm{Co}}=\rho_{\mathrm{Co}}^{0}=0.0889$ at./Å^3. Thus, the intensity of Co is

$$I_{\mathrm{Co}}(\theta)=\sigma_{\mathrm{Co}}I_{\mathrm{Co}}^{0}(\theta)=\sigma_{\mathrm{Co}}I_{\mathrm{Co}}^{0}(\theta)S\int_{0}^{\infty}\rho_{\mathrm{Co}}e^{-z/\lambda\sin\theta}dz=\sigma_{\mathrm{Co}}I_{0}(\theta)S\lambda\sin\theta\rho_{\mathrm{Co}}(1-e^{-a/\lambda\sin\theta})\ . \tag{7}$$

By using Eqs. (3), (6), and (7), we can determine the normalized intensities D_{Ga} and D_{As} of Ga and As at an angle θ:

$$D_{\mathrm{Ga}}(\theta)=[I_{\mathrm{Ga}}^{0}(\theta)]/[I_{\mathrm{Ga}}^{0}(\theta)+I_{\mathrm{As}}^{0}(\theta)+I_{\mathrm{Co}}^{0}(\theta)] \tag{8}$$

and

$$D_{\mathrm{As}}(\theta)=[I_{\mathrm{As}}^{0}(\theta)]/[I_{\mathrm{Ga}}^{0}(\theta)+I_{\mathrm{As}}^{0}(\theta)+I_{\mathrm{Co}}^{0}(\theta)]\ , \tag{9}$$

where $I_{A}^{0}(\theta)=I_{A}(\theta)/\sigma_{A}$ for each element. This corresponds to the measured intensity of Fig. 7.

For the clean surface where the densities of As and Ga were equal, the ratio of their cross sections, $\sigma_{\mathrm{As}}/\sigma_{\mathrm{Ga}}$, was equal to their measured intensity ratio at any angle, the mean value of which is 1.32 for our experimental conditions. Similarly, the Co signal at the highest coverage and various angles was used to determine the ratio

$$\sigma_{\mathrm{Co}}/\sigma_{\mathrm{Ga}}=[I_{\mathrm{Co}}(a=\infty,\theta)/I_{\mathrm{Ga}}(a=0,\theta)][(\rho_{\mathrm{Ga}}^{0}/\rho_{\mathrm{Co}}^{0})]=0.45\ .$$

At the same time, the reduced intensity for each element relative to the emission of that element for the clean surface, as plotted in Fig. 6, is

$$\ln[I_{\mathrm{Ga}}(a,\theta)/I_{\mathrm{Ga}}(a=0,\theta)]=\ln\{b_{\mathrm{Ga}}/(\lambda\sin\theta-b_{\mathrm{Ga}})[e^{-a/\lambda\sin\theta}-e^{-a/b_{\mathrm{Ga}}}]+e^{-a/\lambda\sin\theta}\} \tag{10}$$

and

$$\begin{aligned}\ln[I_{\mathrm{As}}(a,\theta)/I_{\mathrm{As}}(a=0,\theta)]=\ln\{&(\rho_{\mathrm{As}}^{\mathrm{seg}}/\rho_{\mathrm{As}}^{0})[c_{\mathrm{As}}/(\lambda\sin\theta+c_{\mathrm{As}})][1-e^{-a(1/c_{\mathrm{As}}+1/\lambda\sin\theta)}]\\ &+\rho_{\mathrm{As}}^{\mathrm{sol}}/\rho_{\mathrm{As}}^{0}(1-e^{-a/\lambda\sin\theta})+e^{-a/\lambda\sin\theta}+[b_{\mathrm{As}}/(\lambda\sin\theta-b_{\mathrm{As}})][e^{-a/\lambda\sin\theta}-e^{-a/b_{\mathrm{As}}}]\}\ .\end{aligned} \tag{11}$$

In Figs. 6 and 7 we show the fittings of the normalized intensities [Eqs. (8) and (9)] and the reduced intensities [Eqs. (10) and (11)] to the experimental results. For Ga optimal agreement between experimental results and the fitting was found for the characteristic decay length $b_{Ga}=3$ Å. The same value for b_{Ga} was used for fitting all the profiles. These results indicate that the total quantity of reacted Ga is 0.067 at./Å^2 or the equivalent of 1.1 ML of the GaAs(100) surface. Further, the small magnitude of b_{Ga} supports the observation that epitaxial growth of Co can occur (the Co/GaAs interface sustains a sharp concentration gradient).

For the As fittings, the characteristic decay distance from the free surface of Eq. (4), c_{As}, is the same for all the coverages and the quality of fit is very sensitive to the choice of c_{As}; our best fit is obtained by using $c_{As}=5$ Å. With increasing thickness, the magnitude of ρ_{As}^{seg} decreases as more surface As is dissolved into the bulk ($\rho_{As}^{seg}=0.0084$ at./Å^3 or 9.5 at.% at 80 Å; 0.0075 at./Å^3 or 8.4 at.% at 100 Å; and 0.0052 at./Å^3 or 5.8 at.% at 150 Å). However, Eq. (9) is not very sensitive to the choice of b_{As} which characterizes the thin intermixed region at the buried interface (the contribution from these atoms is very small at these high coverages). Since the surface sensitive photoemission results of Fig. 2 showed that the amount of dissociated As within the probe depth changed very little as the overlayer was completed, we estimate that the value of b_{As} for As is approximately the same as for Ga. The fact that c_{As} is a constant indicates that the decay profile of As at the vacuum surface does not change even though the surface concentration of As diminishes with increasing film thickness.

The optimal value of ρ_{As}^{sol} from the fit is found to be 0.000 24 at./Å^3. If we assume that it represents the solubility of As in polycrystalline Co, then this corresponds to about 0.26 at.% of the overlayer. This is a reasonable solubility for a polycrystalline overlayer.

The fitting for films of thickness 15 Å is not as good as for the thick films, but this can be easily understood in terms of the simplicity of the model: It is not surprising that a film only 15 Å thick with a complex interface and vacuum surface can have a profile different from that expected for bulk system in equilibrium. Likewise, for intermediate coverage, the As content at the surface need not be either the value of the substrate or the solubility limit of As in bulk Co. Finally, the approximation that the overlayer thickness equals the nominal Co coverage is poor for very thin films because of the disruption of the substrate.

SUMMARY

In summary, we have found that Co overlayers weakly order as a metastable bcc phase and at the same time promote outdiffusion of both Ga and As. The chemical environments for As and Ga in Co overlayer change with both coverage and distance from the interface. Gallium atoms are concentrated near the interface. Arsenic atoms exhibit a double decay profile, away from the buried interface and from the free surface, and only a small quantity remains dissolved in the Co matrix. These results are similar to those for Fe/GaAs(001), although the latter system possesses a higher degree of structural regularity while also promoting substrate out-diffusion and surface segregation of As. We also expect analogous profiles to appear near the Fe/GaAs(110) surface, consistent with the persistence to high coverage of As emission for that system.[13]

In general, the results presented here suggest that Co/GaAs and Fe/GaAs differ from most other transition-metal—GaAs systems.[3–5,7,8,20] For the others, there is evidence of reaction-induced disruption and the formation of As-based compounds or interface phases. In these cases, the energetics of reaction favor the formation of As-based phases at the interface—not the simpler dissolving of disrupted As atoms in the overlayer matrix as observed here. When that is the case, the density profile is more complicated, but is presently under investigation. For Co/GaAs and Fe/GaAs, we find that epitaxy is favored, even in the presence of limited substrate disruption. At the same time, the behavior observed here for Ga is very similar to that observed for other GaAs interfaces, and we suggest that analogous Ga profiles will be observed away from the buried interfaces for those systems.

ACKNOWLEDGMENTS

The authors are pleased to acknowledge many helpful discussions with Y. Shapira and G. A. Prinz. We are grateful to T.-C. Chiang for generously providing computer codes which served as the starting point for the line-shape decompositions. The synchrotron radiation studies were conducted at the University of Wisconsin Synchrotron Radiation Center, which is supported by the National Science Foundation. This work was supported by the office of Naval Research (N00014-83-K-0579) and the Minnesota Microelectronic and Information Sciences Center.

---

*Permanent address: Brookhaven National Laboratory, Upton, New York 11973.

[1]L. J. Brillson, Surf. Sci. Rep. 2, 123 (1982), and references therein.

[2]*Thin Films—Interdiffusion and Reaction,* edited by J. M. Poate, K. N. Tu, and J. W. Mayer (Wiley-Interscience, New York, 1978).

[3]J. H. Weaver, M. Grioni, and J. J. Joyce, Phys. Rev. B 31, 5348 (1985); M. Grioni, J. J. Joyce, and J. H. Weaver, J. Vac. Sci. Technol. A 3, 918 (1985); M. W. Ruckman, M. del Giudice, J. J. Joyce, and J. H. Weaver, Phys. Rev. B 33, 2191 (1986); J. H. Weaver, M. Grioni, J. J. Joyce, and M. del Giudice, *ibid.* 31, 5290 (1985); M. Grioni, J. J. Joyce, and J. H. Weaver, *ibid.* 32, 962 (1985); M. Grioni, M. del Giudice, J. J. Joyce, and J. H. Weaver, J. Vac. Sci. Technol. A 3, 907 (1985).

[4]P. Oelhafen, J. L. Freeouf, T. S. Kuan, T. N. Jackson, and P. E. Batson, J. Vac. Sci. Technol. B 1, 588 (1983).

[5]W. E. Spicer, P. W. Chye, P. R. Skeath, C. Y. Su, and I. Lindau, J. Vac. Sci. Technol. **16**, 1422 (1979); **17**, 1019 (1980); M. D. Williams, T. Kendelewicz, R. S. List, N. Newman, C. E. McCants, I. Lindau, and W. E. Spicer, J. Vac. Sci. Technol. B **3**, 1202 (1985); T. Kendelewicz, M. D. Williams, W. G. Petro, I. Lindau, and W. E. Spicer, Phys. Rev. B **32**, 3758 (1985); T. Kendelewicz, W. G. Petro, S. H. Pan, M. D. Williams, I. Lindau, and W. E. Spicer, Appl. Phys. Lett. **44**, 113 (1984); J. Nogami, M. D. Williams, T. Kendelewicz, I. Lindau, and W. E. Spicer, J. Vac. Sci. Technol. A **4**, 808 (1986).

[6]G. LeLay, Surf. Sci. **132**, 169 (1983); G. W. Rubloff, *ibid.* **132**, 268 (1983).

[7]R. Ludeke, Surf. Sci. **132**, 143 (1983); G. Landgren, R. Ludeke, Y. Jugnet, J. F. Morar, and F. J. Himpsel, J. Vac. Sci. Technol. B **2**, 351 (1984); R. Ludeke, D. Straub, F. J. Himpsel, and G. Landgren, *ibid.* **4**, 874 (1986).

[8]W. E. Spicer, S. Egglash, I. Lindau, C. Y. Su, and P. R. Skeath, Thin Solid Films **89**, 447 (1982).

[9]G. A. Prinz and J. J. Krebs, Appl. Phys. Lett. **39**, 397 (1981); C. Vittoria, F. J. Rachford, J. J. Krebs, and G. A. Prinz, Phys. Rev. B **30**, 3903 (1984).

[10]G. A. Prinz, Phys. Rev. Lett. **54**, 1051 (1985).

[11]K. Schroder, G. A. Prinz, K.-H. Walker, and E. Kisker, J. Appl. Phys. **57**, 3669 (1985); G. A. Prinz, E. Kisker, H. B. Hathaway, K. Schroder, and K.-H. Walker, *ibid.* **57**, 3024 (1985).

[12]J. R. Waldrop and R. W. Grant, Appl. Phys. Lett. **34**, 630 (1979).

[13]M. W. Ruckman, J. J. Joyce, and J. H. Weaver, Phys. Rev. B **33**, 7029 (1986).

[14]S. A. Chambers, F. Xu, H. W. Chen, I. M. Vitomirov, S. B. Anderson, and J. H. Weaver, Phys. Rev. B **34**, 6605 (1985).

[15]G. Margaritondo, N. G. Stoffel, and J. H. Weaver, J. Phys. E **12**, 602 (1979).

[16]S. A. Chambers and L. W. Swanson, Surf. Sci. **131**, 385 (1983).

[17]J. H. Weaver, Physics Today **39**(1), 24 (1986). The cover photograph shows the spectrometer.

[18]T. Miller and T.-C. Chiang, Phys. Rev. B **29**, 7034 (1986).

[19]M. Grioni, J. J. Joyce, and J. H. Weaver, J. Vac. Sci. Technol. A **4**, 965 (1986). See also J. Nogami, T. Kendelewicz, I. Lindau, and W. E. Spicer, Phys. Rev. B **34**, 669 (1986).

[20]Thermochemistry for the Fe-Ga and Co-Ga systems indicates heats of formation for FeGa to be -18 kJ/mol compared to -31 kJ/mol for CoGa.

[21]This led to the troubling observation that the rate of attenuation of substrate As was slower than that of substrate Ga when, in fact, they must be the same. The detection of a distinct feature at $+0.2$ eV resolved the issue.